ORIGINAL ARTICLE

Cytometry
PART A
Journal of the
International Society for
Analytical Cytology

Some New Faces of Membrane Microdomains: A Complex Confocal Fluorescence, Differential Polarization, and FCS Imaging Study on Live Immune Cells

Imre Gombos,[1] Gábor Steinbach,[2] István Pomozi,[3] Andrea Balogh,[1] György Vámosi,[4] Alexander Gansen,[5] Glória László,[1] Győző Garab,[2] János Matkó[1]*

[1]Department of Immunology, Institute of Biology, Eotvos Lorand University, Budapest, Hungary

[2]Biologial Research Center, Hungarian Academy of Sciences, Szeged, Hungary

[3]Pi Vision Partnership, Budapest, Hungary

[4]Cell Biophysics Group of the Hungarian Academy of Sciences, University of Debrecen, Debrecen, Hungary

[5]Division Biophysics of Macromolecules, German Cancer Research Center, Heidelberg, Germany

*Correspondence to: Janos Matko, Department of Immunology, Institute of Biology, Eotvos Lorand University, Budapest, Hungary.

Email: matko@elte.hu

ISAC
International Society for Analytical Cytology

• **Abstract**

Lipid rafts are cholesterol- and glycosphingolipid-rich plasma membrane microdomains, which control signal transduction, cellular contacts, pathogen recognition, and internalization processes. Their stability/lifetime, heterogeneity remained still controversial, mostly due to the high diversity of raft markers and cellular models. The correspondence of the rafts of living cells to liquid ordered (Lo) domains of model membranes and the effect of modulating rafts on the structural dynamics of their bulk membrane environment are also yet unresolved questions. Spatial overlap of various lipid and protein raft markers on live cells was studied by confocal laser scanning microscopy, while fluorescence polarization of DiIC18(3) and Bodipy-phosphatidylcholine was imaged with differential polarization CLSM (DP-CLSM). Mobility of the diI probe under different conditions was assessed by fluorescence correlation spectroscopic (FCS). GM1 gangliosides highly colocalized with GPI-linked protein markers of rafts and a new anti-cholesterol antibody (AC8) in various immune cells. On the same cells, albeit not fully excluded from rafts, diI colocalized much less with raft markers of both lipid and protein nature, suggesting the Lo membrane regions are not equivalents to lipid rafts. The DP-CLSM technique was capable of imaging probe orientation and heterogeneity of polarization in the plasma membrane of live cells, reflecting differences in lipid order/packing. This property—in accordance with diI mobility assessed by FCS—was sensitive to modulation of rafts either through their lipids or proteins. Our complex imaging analysis demonstrated that two lipid probes—G_{M1} and a new anti-cholesterol antibody—equivocally label the membrane rafts on a variety of cell types, while some raft-associated proteins (MHC-II, CD48, CD59, or CD90) do not colocalize with each other. This indicates the compositional heterogeneity of rafts. Usefulness of the DP-CLSM technique in imaging immune cell surface, in terms of lipid order/packing heterogeneities, was also shown together with its sensitivity to monitor biological modulation of lipid rafts. © 2007 International Society for Analytical Cytology

• **Key terms**

lipid rafts; live lymphoid cells; confocal polarization imaging; FCS; raft modulation

MICRODOMAINS enriched in cholesterol and glycosphingolipids (so called lipid rafts) are expressed in the plasma membrane of most mammalian cells (1–6) and involved in numerous membrane-associated cellular functions. Compartmentation, spatiotemporal coordination and coupling or isolation of receptor-, signal-transducing, or regulatory proteins were shown to be controlled, in some ways, by lipid rafts (3–6). Furthermore, these microdomains are supposed to be involved in the capturing and internalization of some viruses (e.g. human immunodeficiency virus, HIV and influenza virus), bacteria, or bacterial inflammatory molecules (e.g. toxins or lipopolysaccharides) by host cells (6,7) in the immune system and in regulation of

signal transduction in neuronal synapses (8). Moreover, a correlation between cholesterol homeostasis and appearance/composition of membrane microdomains in human monocyte-macrophage cells (9), as well as a differential regulatory role of E-LDL and Ox-LDL in the cholesterol- and ceramide-rich microdomains of these cells have recently been shown (10). Thus, lipid raft and caveola membrane microdomains gained a widespread attention in the research of cellular communication and signal transduction in general, and in the immunological, virological, and neurobiological research areas in particular.

Despite the extensive biochemical and biophysical characterization on model membranes and cells, several basic properties of these membrane microdomains on live cells (e.g. size, stability, fine structure, or compositional diversity), as well as the regulatory mechanisms controlling these properties still remained controversial and less understood (2,6,11–13). Since there is an ongoing debate on the size, size-distribution, lifetime and stability of microdomains, many groups are devoted to characterize different aspects of rafts by using various versions of optical fluorescence or scanning probe imaging. These approaches, focusing mostly on model membranes with less complexity, include, among others, confocal fluorescence (FRET-) microscopy (11); single particle tracking video-imaging (13); fluorescence correlation (FCS) microscopy (14,15); two-photon microscopic imaging of laurdan generalized polarization domains (16) and atomic force imaging of model membranes (17,18).

Various probes are used to mark these microdomains, such as fluorescent antibodies against GPI-anchored proteins (e.g. CD48, CD55, CD59, CD14, HA-R, AP, FR, etc.), GPI-GFP reporters, the cholera toxin β subunit binding selectively to $G_{M1,3}$ gangliosides or fluorescent lipid analogs (6). We have recently developed new IgG type monoclonal antibodies reactive to clustered cholesterol in both cell-free systems, such as lipoproteins, and in live immune cells (e.g. lymphocytes, macrophages). These antibodies were shown capable of marking cholesterol-rich membrane microdomains (rafts or caveolas) or even their redistribution in the plasma membrane of activated lymphocytes (19).

The phase separation of Lo (liquid ordered) and Ld (liquid disordered, fluid) domains has been quite extensively studied earlier in various model membrane systems (6,20–22). The imaging studies on such systems often applied fluorescent lipid probes to mark these domains, such as the diIC18 or diIC20 indocarbocyanine probes (diI) for Lo domains or Bodipy-phosphatidylcholine (B-PC) for the Ld domains (20–22). Although lipid rafts are often depicted as ordered lipid domains, the diI probe, partitioning well into Lo domains in model membranes of simple composition (e.g. GUVs) (20), has been assumed as a non-raft lipid probe (23,24), based on its weak miscibility with sphingomyelin (SM)-enriched regions. In these GUV (Giant Unilamellar Vesicle) models cholesterol was shown to increase separation of the Lo and Ld phases in a concentration dependent manner, demonstrating its capability to fine-tune dynamics of membrane phases and microdomains. The question whether the phase-relations and

raft dynamics is similar in the plasma membrane of live cells, however, is still debated (24).

The lateral contacts of raft microdomains to their neighboring membrane areas, as well as the domain boundaries of Lo phase regions are both poorly understood in live cells. In order to investigate these questions we applied here a recently introduced novel differential polarization laser scanning confocal microscopic approach (DP-CLSM) (25,26) to further analyze the ordering of plasma membranes and lipid packing of live lymphoid cells. For this purpose we used the aforementioned indocarbocyanine lipid probe, diIC18(3). The expected membrane perturbation caused by this probe is certainly lower than those appearing when a large fluorescent IgG antibody, the very specific, but pentameric polypeptide, CTX-B, or large immunogold labels are used. Moreover its dipole orientation relative to the membrane surface was experimentally established and shown to be preferentially tangential, at least in red blood cells (27). Therefore it seems a suitable probe to study changes of lipid order/packing and the effects of raft modulations on their lipid neighborhood in live cells.

In the present study we addressed the following questions: (i) to what extent does the new marker of clustered cholesterol (AC8 antibody) overlap with $G_{M1,3}$ ganglioside-enriched domains and with the diI lipid probe in a variety of live immune cells; (ii) to what extent do the different protein markers of rafts overlap with the above two lipid probes and with each other; (iii) what can the differential polarization (DP-CLSM) images of diI tell us about lipid raft dynamics and the coupling of rafts with their lipid neighborhood. Our data demonstrate that cholera toxin B and the new anti-cholesterol antibody, AC8, as two lipid probes of membrane rafts, show a highly matching membrane localization in all cell types investigated, confirming that the gangliosides and cholesterol may indeed form a stable "nucleus/molecular skeleton" for membrane rafts. In contrast, several raft-associated proteins (e.g. MHC-II, CD48, or CD90) show a differential colocalization, reflecting a compositional heterogeneity in the protein content of co-existing lipid rafts on live immune cells. Usefulness of the differential polarization CLSM method in imaging immune cell surface in terms of lipid order/packing heterogeneities and detection of biological modulation of lipid rafts are also demonstrated and discussed.

MATERIALS AND METHODS

Cells and Reagents

The human Kit225 K6 T-lymphoma cell line (kindly provided by T.A. Waldmann, Bethesda, MD) was cultured in RPMI 1640 medium supplemented with 10% fetal calf serum (FCS), penicillin, streptomycin, Na_2CO_3, and sodium pyruvate. Recombinant IL-2 (20 U/ml) was added in every 48 h (28). For the experiments, cells were harvested, washed, and resuspended in PBS, pH 7.4. JY human B lymphoblasts (HLA-A2,B7+) (29) were grown in RPMI 1640 + 10% FCS medium, while 2PK3 (I-Ed +, I-Ad +) murine B-lymphoma cell line of BALB/c origin (ATCC, TIB-203) and the L929 C3H/An mouse fibroblasts (ATCC, CCL-1) were cultured in RPMI

1640 medium with 0.05 mM 2-mercaptoethanol and 5% FCS, in 5% CO_2 atmosphere, at 37°C (30). Ten-week-old male Sprague-Dawley rats were decapitated, hearts were removed, rinsed in isotonic saline solution (0.9% NaCl), blotted dry, and chambers were separated from each other. Left ventricular tissue samples were sliced and stained right before they were assayed.

MβCD and MγCD (random methylated β and γ cyclodextrin) was purchased from CycloLab (Budapest, Hungary). Alexa 488-(or 647-) cholera toxin B, diIC18(3) and Bodipy-phosphatidylcholine were obtained from Molecular Probes-Invitrogen (Eugene, OR). MEM-75 (against transferrin receptor/CD71) and MEM-102 (against CD48) mAbs were kindly provided by V. Horejsi (Institute of Immunogenetics, ASCR, Prague, Czech Republic) and they were conjugated with Alexa fluorophores according to the manufacturer's instructions (Molecular Probes-Invitrogen).

Cell Labeling

Cells were labeled with Alexa488-conjugated cholera toxin B according to the manufacturer's (Molecular Probes-Invitrogen) instruction. Staining with diI (1.5 μg/ml) was performed by incubating the cells for 2–3 min., at 37°C, in HBSS (+5 mM glucose + 1% BSA), using a sonicated, air-fuged, and filtered stock solution of diI in ethanol. In case of double labeling, cells were incubated sequentially in diIC18(3) and then CTX-B for 10 min on ice. Cells were labeled with fluorescent antibodies for 40 min, on ice, and then washed twice before measurement. Human CD71 specific Cy3-MEM-75 (mouse IgG1 Ab) and FITC-conjugated rat anti-mouse antibody G7.4 (IgG2c, from ATCC) was used to label transferrin receptor and Thy1 (CD90), respectively. CD2 on T-cells were labeled with FITC-conjugated anti-human CD2 mAb (Sigma, St. Louis, MO, USA). ACHAs were applied either as Alexa488-conjugated AC8 or biotinylated AC8 followed by Alexa647-conjugated neutravidin and the cells were stained as described recently (19). In case of double labeling, the lipid probes and the antibodies were usually added to the cells simultaneously for the appropriate time intervals. No competition or mutual blocking of binding was observed with any pairs. For the fluorescent antibodies appropriate isotype control antibodies (or cell lines) were used as negative controls.

Depletion of Membrane Cholesterol by MβCD

Freshly harvested cells (1 × 10⁶/ml) were incubated with 10 mM MβCD or MγCD (control) (Cyclolab, Budapest, Hungary) for 15 min, at 37°C, in PBS pH 7.4 and then washed. Forty to fifty percent of plasma membrane cholesterol could be removed with this treatment (28). MγCD a conformational isomer incapable of cholesterol extraction was used as control. After washing, the cells were labeled accordingly for further analysis.

Membrane Modulation by Crosslinking of Membrane Proteins

Cells were incubated with unconjugated MEM-75 (reactive with transferrin receptor, CD71) or MEM-102 (reactive with CD48) monoclonal antibodies on ice, for 40 min. After

washing, samples were incubated with polyclonal goat anti mouse IgG for 30 min, on 37°C, to crosslink the primary antibodies.

CLSM Measurements

The stained cells or tissue sections were mounted on coverslip and imaged by Olympus FluoView500 confocal laser scanning microscope, using the 488 nm argon-ion laser line to excite Alexa 488 dye and the 543 nm He-Ne laser line for the diIC18(3). In case of long wavelength probes, a 632 laser line (He-Ne) was applied. The images (512 × 512 pixels) were recorded by using a 60× oil-immersion objective (N.A.:1.25). An SDM560 dichroic mirror and a BA505-525 bandpass emission filter was used for detecting Alexa 488 fluorescence (channel 1), SDM630 dichroic mirror and BA560-600 bandpass filter was used in channel 2 for detecting diIC18(3) emission and a 660IF long pass filter was used in channel 3 for detecting the fluorescence of long-wavelength probes Cy5 or Alexa647. A sequential scanning mode was applied in colocalization experiments to minimize the crosstalk between channels.

Pearson's colocalization coefficients were calculated by using the ImageJ software. The same experimental setup and strategy was applied to investigate colocalization of various double-stained lymphoid cells by CLSM.

FRET Measurements

FRET between membrane proteins, after their fluorescent immunocytochemical labeling, was measured either by the acceptor photobleaching FRET or the intensity-based FRET method (31). FITC-Cy3, Cy3-Cy5, or Alexa546-Cy5 dye pairs served as donors and acceptors, respectively. FRET efficiencies were measured by recording 512 × 512 pixels images of the double- or single (donor- or acceptor-) labeled cells in the optical channels of the FluoView 500 CLSM system, selected properly for the given dye pair by the appropriate emission filter combinations and dichroic mirrors. The images were evaluated for FRET efficiency as described previously (31,32).

FCS Measurements

FCS measurements were carried out on the fluorescence fluctuation microscope (FFM) constructed by Prof. Jörg Langowski's group at the DKFZ, Heidelberg. The setup combines an FCS/FCCS module with a galvanometric laser scanner attached to the video port of an inverted IX-70 microscope (Olympus, Hamburg, Germany) with a UplanApo 60×, 1.2 NA water immersion objective (33,34). Measurements were performed at room temperature. DiI fluorescence was excited with the 568 nm line of an Ar-Kr laser from Omnichrome (Wessling, Germany). Emission was detected through a 590–750 nm bandpass filter (OG590+700CSFP, Omega Optical, Brattlerborn, VT) by an avalanche photodiode (SPCM-AQR-13, Perkin-Elmer, Wellesley, MA). Confocal images of the cell membrane were acquired, and the laser beam was positioned at selected points of the membrane for FCS measurements. Laser power at the objective was ∼ 0.8 μW. For calculating the autocorrelation function from the signal of the photodiode, an ALV-5000/E correlator card (ALV Laser GmbH, Langen,

Germany) was used. Data acquisition time was always 60 s, corresponding to 10 runs of 6 s, which were averaged. From each sample ∼10 cells were measured. Autocorrelation functions were fitted to a single component 2D diffusion model with triplet term using the program QuickFit (written in the laboratory of J. Langowski, DKFZ, Heidelberg):

$$G(\tau) = \frac{1}{N} \frac{\left(1 - T + Te^{-\tau/\tau_{tr}}\right)}{1 - T} \left[\left(1 + \frac{\tau}{\tau_d}\right)^{-1}\right],$$

where N is the average number of molecules in the detection volume, T is the fraction of diIC18(3) molecules being in the triplet state within the detection volume, τ_{tr} is the phosphorescence lifetime of diIC18(3) and τ_d is the diffusion time, which is the average time spent by the dye in the detection volume. The diffusion coefficient, D can then be derived as: $D = \omega_{xy}^2/4\tau_D$, where ω_{xy} is the lateral radius of the sensitive volume. ω_{xy} at 568 nm excitation was estimated by measuring the diffusion time of Alexa Fluor 568 dissolved in PBS ($\tau_d = 60 \pm 2$ μs at 25°C). Assuming inverse proportionality between the MW and D, and using Rhodamine 6G as reference (Culbertson et al., 2002, Talanta 56:365), we assessed the diffusion coefficient of Alexa Fluor 568 as $D_{Alexa\ 568} \sim D_{R6G} \times MW_{R6G}/MW_{Alexa\ 568} = 4.14 \times 10^{-6}$ cm²/s × 471/716 = 2.72 × 10⁻⁶ cm²/s. From this the radius was estimated to be $\omega_{xy} = \sqrt{4D\tau_D} \sim 255 \pm 5$ nm.

Differential Polarization Laser Scanning Microscopy

For recording P (the degree of polarization of the fluorescence emission) images we used a Zeiss LSM 410 laser scanning microscope equipped with DP (differential polarization) attachments. The overall schemes and technical details, including calibration and correction procedures, taking into account the polarization characteristics of the dichroic beam splitter, have been published elsewhere (25,26). For P imaging of the lymphocyte cells in the DP-CLSM (differential polarization confocal laser scanning microscope), the sample was excited with either the 488 or 514 nm linearly polarized beams of an Ar-ion laser. The polarization content of the fluorescence emission was analyzed with the aid of a photoelastic modulator (PEM, Hinds International) and a demodulation circuit, which consisted of a programmable, gated digital phase-sensitive detector (DPSD) constructed by Pawel Kamasza (SZFKI KFKI, Budapest). The DPSD was locked at the modulation frequency of PEM, at 100 kHz, and a low pass analog-digital converter amplifier (ADC) was used to determine the average intensity, I_a. The analyzer unit was adjusted in a manner to detect the intensity difference $\Delta I = I_1 - I_2$, where the polarized components are parallel (I_1) and perpendicular (I_2) to the polarization direction of the laser beam. P was calculated as $\Delta I/2I_a$, with $I_a = (I_1 + I_2)/2$.

5×10^5 Kit225 K6 T-lymphoma or JY human B lymphoma cells suspended in PBS were labeled with diIC18(3). After washing, cells were resuspended in PBS and mounted on coverslip. The 514 nm laser line was used for excitation, an FT560 dichroic beamsplitter and an additional long pass 560 nm color filter was used to separate the fluorescence; the PEM was adjusted to 586 nm, which is the emission peak of diIC18(3). When labeling with Bodipy-phosphatidylcholine, cells were incubated at the same density with the probe (1.5 μg/ml) for 10 min, at room temperature. After washing, cells were mounted on coverslip. Excitation of Bodipy fluorescence was at 488 nm, using an FT510 beamsplitter and a long pass 510 nm filter; PEM was adjusted to the emission peak (520 nm) of Bodipy-PC.

RESULTS

Staining Patterns of the Fluorescent Lipid Membrane-Probes on Live Lymphoid Cells

In earlier studies the large diversity of the applied, supposed raft markers, and cellular models resulted in a broad spectrum of their localization and physicochemical properties (6). Therefore here we tried to perform a systemic study on cell types phenotypically closely related to each other, such as T- and B-lymphoma cells of human or murine origin and to apply the same lipid raft markers to all. First, we tested how the staining pattern of these cells with various well defined markers of lipid rafts (e.g. CTX-B, a new anti-cholesterol antibody, AC8) or with diIC18(3) and Bodipy-PC, lipid probes of Lo and Ld phase domains, respectively (12,20,21). As the representative intensity surface plots on Figure 1 show, the human T lymphoma cells (Kit 225 K6) displayed a differential staining pattern with these probes. While CTX-B, AC8, and diIC18(3) all stained these cells in a pattern of discrete small patches (Figs. 1A–1C), while the Bodipy-PC probe, enriched in the fluid membrane regions, as expected, stained the plasma membrane more homogenously (Fig. 1D). Similar staining patterns were observed for these probes in human B lymphoblast (JY) and macrophage (U937) cell lines (data not shown).

Membrane Domains Defined by diIC18(3) Match the Domains of Classical Lipid Raft Markers Only Partially in Lymphoid Cells

Despite that diIC18(3) was defined by model membrane studies as nonraft marker (enriched in Lo phase domains) (23,24), showed a typical patchy staining pattern on the surface of lymphoid cells (see Fig. 1C), suggesting that these 200–300 nm diameter patches define a certain type of membrane microdomain in these cells. A substantial colocalization was found between the new fluorescent AC8 anti-cholesterol antibody (19), and the CTX-B labeled G_{M1} gangliodies, the classical markers of rafts. A high level of matching of the AC8-labeled and G_{M1}-CTX-B + domains was observed in both B- and T-lymphocytes of human origin (cross correlation (cc): 0.68 and 0.67, respectively), similarly to murine T_H cells and macrophages (Table 1). The colocalization between diIC18(3) and AC8, however, was significantly lower (cc: 0.4) in the same cells. The spatial correlation between diIC18(3) and the G_{M1}/CTX-B domains was the lowest (28–34%), as assessed by a CLSM analysis on cells of different origin (Figs. 1E–1H), and it was independent of the cell type. These data suggest, that the "clustered" cholesterol and G_{M1} have a high spatial correlation in all cell types investigated, but the membrane regions
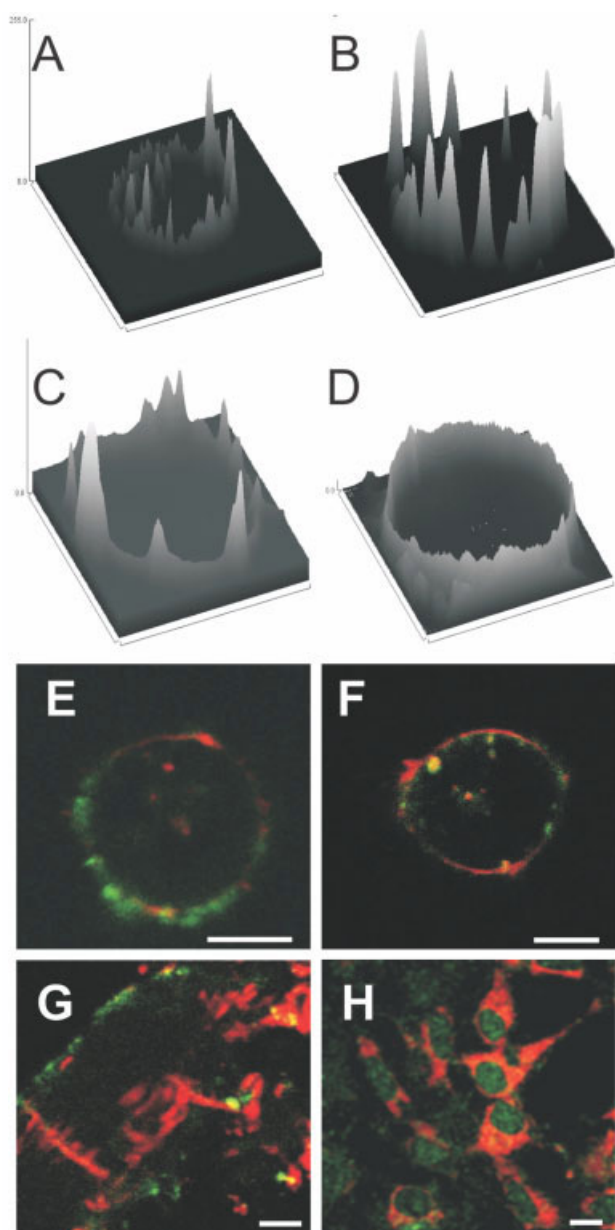
Figure 1. Staining pattern of various lipid probes on human T lymphoma cells and the colocalization of diIC18(3) with cholera toxin B on various cell types. Alexa488-Cholera toxin B labeling GM$_{1,3}$ gangliosides (**A**), Alexa488-AC8 anticholesterol antibody (**B**) and diIC18(3) (**C**) all stained Kit225 K6 T cells in a patchy fashion, defining discrete microdomains. Membrane staining by Bodipy-C5-phosphatidylcholine of the same cells (**D**) is much more homogenous. The fluorescence intensity surface plots were derived from representative confocal microscopic equatorial optical sections (width: 0.3 μm) recorded by a 60× oil immersion objective (N.A. 1.25). Colocalization of Alexa488-CTX B with diIC18(3) is shown on 2PK3 murine B lymphoma (**E**), JY human B lymphoblast (**F**), left ventricular tissue sections of raft heart (**G**), and L929 murine fibroblast (**H**) cells. The images were recorded by confocal microscope as described earlier, the white bars indicate 10 μm. The colocalization indices were 0.30 ± 0.12 (E), 0.34 ± 0.1(F), 0.26 ± 0.12 (G), and 0.32 ± 0.18 (H), respectively.

defined by diIC18(3) have a poor, but still non-negligible overlap with lipid rafts labeled with these two markers, on cells of lymphoid origin.

Lipid Rafts of Lymphoid Cells' Plasma Membrane Show Some Compositional Heterogeneity

Among the GPI-anchored lipid raft marker proteins, CD90 and CD59 are found mostly in T cells, while CD48 is expressed on both T and B cells of lymphoid origin (4,6). In contrast, CD2 is an abundant nonraft protein in T cells (35). Key molecules of antigen presentation, the class I and class II major histocompatibility antigens (MHC-I, MHC-II) are expressed on both T- and B-lymphoma cells and a substantial fraction of MHC-II was shown raft-associated on these cells (30,36). Here we tried to map the mutual colocalization/proximity of these membrane proteins with each other and with the aforementioned lipid markers of raft domains, using CLSM/FRET and colocalization analysis. As expected, CD48 and CD90 are firmly associated with the membrane domains defined by both G$_{M1}$/CTX-B and the anti-CHOL antibody, AC8 (19), while the nonraft CD2 protein did not associate with these domains (Table 1).

Concerning the MHC glycoproteins, colocalization and FRET data consonantly show that MHC-II is associated with raft marker G$_{M1}$, in a much higher extent than MHC-I, in the B- and T-lymphoma cells (Table 1). In addition, earlier data have shown that MHC-II is partially detergent resistant and that its homoassociation (clustering) on murine B lymphoma cells was cholesterol-sensitive (30). In contrast, MHC-I clusters on B lymphoma cells proved to be less sensitive to cholesterol, but rather dictated by β2m-dependent protein–protein affinity (37), consistent also with their very weak association with the G$_{M1}$/CTX-B-rich domains.

Despite its raft-association, MHC-II molecules show rather weak if any colocalization/proximity with CD48. A somewhat stronger colocalization with CD59 was observed on the same cells. Taking these data together, the MHC-II enriched lipid rafts of B and T lymphoma cells seem to be separate microdomains from those enriched in CD48, but show some degree of mutual compartmentalization with CD59. This can be regarded as a piece of evidence for heterogeneity in protein-composition of lipid rafts in lymphoid cells.

P-Imaging of diI-Stained Lymphoid Plasma Membranes with Differential Polarization Microscopy

By combining the technique of differential polarization (DP) with confocal microscopy a method has become available for imaging not only the fluorescence intensity but also the polarization or anisotropy DP parameters. For linearly polarized light, these include *P*, the degree of polarization of the fluorescence emission, which characterizes the depolarization e.g. due to rotation of the molecules and/or due to excitation energy transfer or migration in the system, linear dichroism (LD) and fluorescence detected LD, which are given rise by the anisotropic distribution of the absorbance dipoles, and *r*, the anisotropy of the fluorescence emission, a quantity which originates from the nonrandom distribution of the

Table 1. Colocalization/proximity of some membrane microdomain constituents in lymphoid cells

MEMBRANE MOLECULE I	MEMBRANE MOLECULE II	CELL TYPE	COLOCALIZATION INDEX	FRET EFFICIENCY (%)	REFS.[a]
GM_1 (CTX-B)	AC8 mAb	Murine T_H-cells, macrophages	0.65 ± 0.01	n.d.	(19)
GM_1 (CTX-B)	CD48	Kit225 K6, T_H-cells	0.64 ± 0.02	0.29 ± 0.06	
GM_1 (CTX-B)	CD48	Kit225 K6, T_H-cells (CHOL-depleted)	0.17 ± 0.01	0.06 ± 0.01	
GM_1 (CTX-B)	CD2	Kit225 K6, T_H-cells	0.04 ± 0.02	n.d.	
AC8 mAb	Thy.1(CD90)	Murine T_H cells	0.56 ± 0.09	n.d.	(19)
AC8 mAb	CD2	Murine T_H cells	0.06 ± 0.03	n.d.	(19)
MHC-I/β2-microglobulin	GM_1 (CTX-B)	JY B-, Jurkat T-lymphoma cells	0.11 ± 0.04	0.09 ± 0.04	
MHC-II	GM_1 (CTX-B)	JY B-, Jurkat T-lymphoma cells	0.54 ± 0.05	n.d.	
MHC-II	CD48	JY B-, Jurkat T-lymphoma cells	0.1 ± 0.06	0.07 ± 0.03	
MHC-II	CD59	JY B-, Jurkat T-lymphoma cells	0.37 ± 0.07	n.d.	

[a]Some data from our recent work published in Ref. 19 are given for comparison.

emission dipoles with respect to a coordinate system fixed to the laboratory or the sample (26).

We applied diIC18 and Bodipy-PC to probe Lo and fluid membrane regions (Fig. 2A) on live cells by DP-CLSM. As shown by Axelrod et al. (27) on red blood cells, the long fatty acyl chains of diIC18(3) are aligned preferentially parallel with the membrane normal, keeping the orientation of the indocarbocyanin's absorption dipole uniformly tangential with respect to the surface of the plasma membrane. In perfect accordance with the expectations, diIC18(3) probe shows a similar orientational behavior in both B and T lymphoblastoid cells (JY and Kit225 K6, respectively). In microscopic samples containing nonrandom orientation of the emission dipoles, i.e. in samples which exhibit nonzero r, P contains information both on the anisotropic distribution of the emission dipoles with respect to the membrane plane and on the depolarization due to the motional freedom of the lipid-dye molecular assemblies. This is demonstrated by the color-coded P-images of JY cells, which in the vertical and horizontal directions are dominated by the preferentially parallel and perpendicular orientation of the emission dipoles, resulting in positive and negative P values, respectively (Fig. 2B). (Note: in macroscopic samples this information is lost due to spatial averaging; in highly anisotropic samples, however, P might contain contributions from the residual anisotropy e.g. due to photoselection and/or due to gravitational alignment of the particles (38)).

In contrast to diIC18, Bodipy-PC is preferentially inserted into the fluid (Ld) regions of the plasma membrane through much shorter fatty acyl chains and the fluorophore ring is attached only to one of them. Thus, its absorption dipole is expected to be aligned in a less ordered fashion with respect to the membrane surface. The color-coded representative P-images of B-PC in JY B cells (Fig. 2B) indeed show that B-PC fluorescence is much less polarized throughout the membrane surface than that of the diIC18. Interestingly, as shown by the intensity and P-images of diIC18 recorded on membrane cholesterol-depleted JY cells, the diI staining became less patchy/more uniform, but a few large diI clusters are formed on the cells. The averaged P values became lower upon cholesterol depletion.

A large scale statistical analysis of Bodipy-PC and diIC18 P-images recorded on large human T lymphoma cells (Kit225 K6) resulted in similar, heterogenous P-distributions (Fig. 3). These distributions correspond to spatial averaging, at least for the selected sections, and thus the mean values can be compared with macroscopic measurements. The Bodipy-PC P-histogram is quite narrow, and at the same time the mean value (0.09) is rather small. This reflects a highly depolarized emission from Bodipy-PC all over the cells, and indicates a high rotational freedom with respect to the membrane normal and small contribution from r. In contrast, the diIC18(3) P-histograms are significantly broadened due to large contributions from the anisotropic distribution of the emission dipoles with respect to the membrane planes, and inhomogeneities in the local microenvironment of the probe over the cell surface. This difference is consistent with the intensity surface plots of the probes (see Figs. 1C and 1D).

Depletion of membrane cholesterol slightly decreased the width of P-distribution and shifted its mean value toward 0, consistent with results of macroscopic steady-state polarization data with DPH probes on the same Kit225 K6 T cells (28). Extensive crosslinking of either raft-associated CD48 GPI-anchored proteins or a nonraft protein, the transferrin receptor (CD71) both resulted in a significant positive shift in the mean value of P-distributions (smaller rotational freedom) of DiIC18(3) in the Kit225 K6 T cells.

FCS Analysis of the Mobility of diIC18(3) in the Plasma Membrane. Effects of Lipid Raft Modulations

The lateral mobility of diIC18(3) was analyzed by fluorescence correlation microscopy (23,33,34) upon various lipid raft modulation treatments in human Kit 225 K6 T lymphoma cells. Typical autocorrelation curves fitted to a single component diffusion model including triplet correction are shown in Figure 4. The average diffusion correlation time (τ_D, determined from 11 cells) was 24.1 ± 13.4 ms for control cells (Fig. 4A) and increased to 33.7 ± 7.8 ms ($n = 12$) upon crosslinking CD48, a constitutively raft-localized membrane protein (Fig. 4C). These values of τ_D correspond to diffusion coefficients of $(6.8 \pm 4) \times 10^{-9}$ cm^2/s and $(4.8 \pm 1.1) \times 10^{-9}$ cm^2/s,
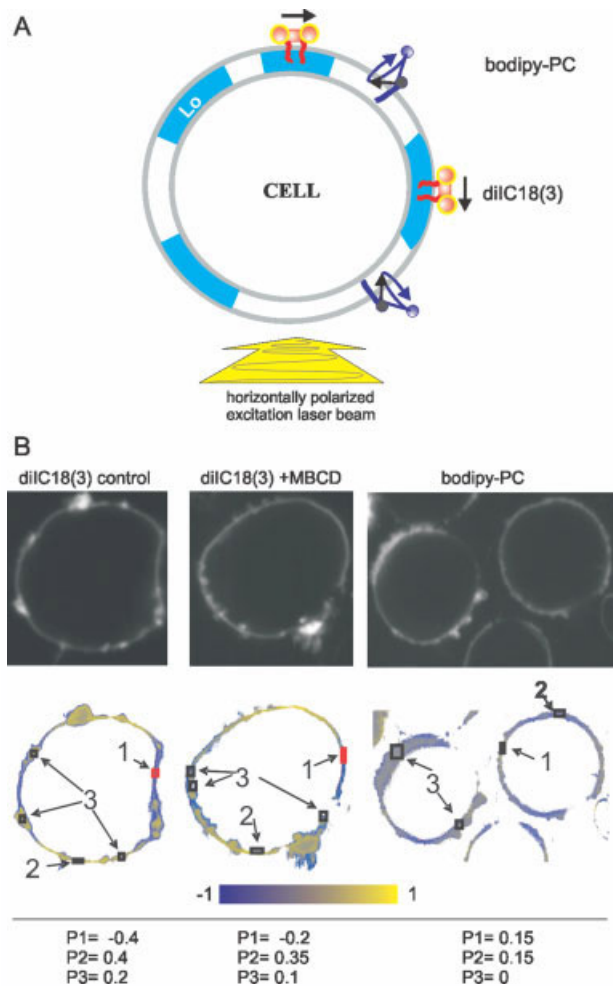
Figure 2. Model system and analysis strategy of P-imaging on live lymphoid cells by DP-CLSM. (**A**) Cells are excited by horizontally polarized laser beam. The scheme shows the preferred (tangential) orientation of diIC18 dipoles with respect to the membrane plane. For Bodipy-PC free conical rotation with respect to the tangential axis is allowed. (**B**) shows the fluorescence (gray scale, upper panels) and P (yellow-blue, lower panels) images of diIC18(3) in control (left), and MBCD-treated (middle) JY cells and the Bodipy-PC stained JY cells (right). In the P patterns the yellow color codes the horizontal, while the blue the vertical dipole orientations; the more saturated the color the higher the P value is; some quantitative P values derived from the numbered ROIs are shown as an example. The indices of P values correspond to the indicated membrane regions: in the diIC18(3) images the dipoles are aligned tangentially to the membrane (horizontal and vertical orientations from horizontal and vertical membrane regions, respectively) with relatively high values, while the P values in the Bodipy-PC image are rather small.

respectively. The average τ_D was even higher, 62.9 ± 42 ms corresponding to $D = (2.6 \pm 1.7) \times 10^{-9}$ cm^2/s ($n = 10$) when cholesterol was depleted from the plasma membrane by MBCD treatment (Fig. 4B). We note here that in some of the cholesterol-depleted cells the diffusion of diIC18 was extremely slowed down ($\tau_D > 100$ ms), while in other cells τ_D was close to that of the control cells, resulting altogether in an elevated average value. These data reflect decreased local diffu-

sion rates of diIC18(3) upon both types of lipid raft modulation in randomly selected membrane areas of T cells.

DISCUSSION

In the present work, first we demonstrated that a new anti-cholesterol antibody (AC8) labeling the clustered cell membrane cholesterol is highly enriched in the membrane domains defined by G$_{M1,3}$ gangliosides (cholera toxin labels) in human B- and T-lymphoid cells. Although quantitative cell surface staining with AC8 can be assessed only by a standard limited papain digestion, snapshot imaging of cells stained by AC8 could monitor not only the level of membrane cholesterol, but even redistribution of rafts in the plasma membrane, such as raft polarization upon T cell activation (19). Thus, G$_{M1,3}$ gangliosides and clustered cholesterol seem to be two essential "nucleating molecular skeletal elements" of lipid rafts existing in various lymphoid (T- and B-lymphocytes) or myeloid (e.g. monocyte-macrophage) cells of the immune system. The strong correlation between CTX-B and AC8 binding (expression) in seven different immune cells (19) indicates that regulation of their expression might be complex and not independent of each other, as proposed recently (9). Their simultaneous application might be a useful tool in a reliable detection of raft (or caveola) microdomains by fluorescence imaging.

Our results have also shown that some protein markers of rafts, such as CD48, CD59, or CD90 GPI-anchored proteins all highly colocalize with both CTX-B and AC8 in B- and T-lymphoid cells of mouse and human origin. On the other hand, these GPI proteins differentially colocalize with each other and with some transmembrane proteins, such as MHC-II or MHC-I glycoproteins. While the MHC-II-enriched raft domains (30,36) do not overlap with the CD48-enriched rafts, some CD59 was found in these MHC-II-clusters. Microcompartmentation of MHC-II by rafts may have important functional consequences, both in controlling the efficiency of antigen presentation (30) or through their raft/dependent and raft/independent signaling pathways (39). Similarly, Fas receptor/CD95 signaling was found differentially regulated, depending on the receptor localization in CD48-rich rafts or CD55-, CD59-rich microdomains (40). These results together provided a piece of evidence for coexisting lipid rafts with protein compositional diversity in lymphocytes. Similar compositional heterogeneity of membrane microdomains was reported on myeloid (monocyte-macrophage) cells (41) and even lipid domains distinct from cholesterol/SM-rich rafts were described on fibroblasts (42). Such compositional heterogeneity of rafts and their differential cellular localization may serve as a compartmentation mechanism providing a tool for spatiotemporal coordination of protein functions in the plasma membrane and various subcellular structures.

A detailed confocal colocalization analysis has also shown that the microdomains defined by both G$_{M1,3}$ gangliosides/CTX-B and the AC8 anti-cholesterol antibody overlap only partially (weakly) with membrane domains defined by the diIC18 probe, proposed as a nonraft marker enriched in Lo phase domains in model membranes (8,12,20–23). This low, but not negligible (20–30%) colocalization of diI with both
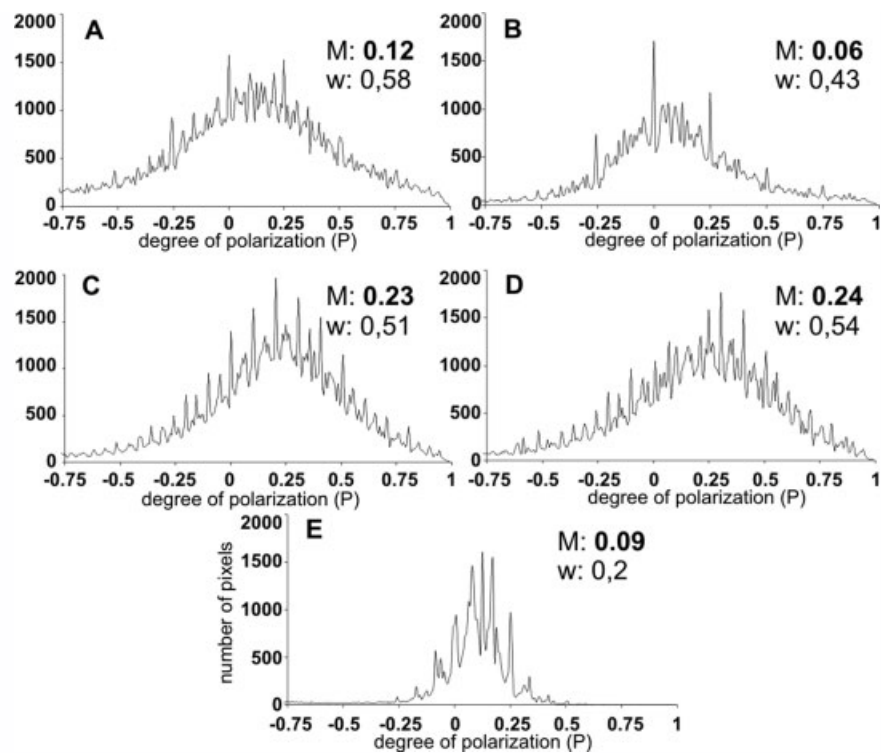
Figure 3. Distribution of *P* values detected for diIC18(3) and Bodipy-PC on Kit225 K6 T lymphoma cells: effect of membrane raft modifications. The *P* values, indicated on the *X* axis, were measured for selected cells (8−10/graph) by recording DP-CLSM images. The *Y* axis shows the normalized number of pixels with a given *P* value. Panels **A**−**D** display diIC18(3) fluorescence *P*-histograms in control, MBCD treated, CD48-crosslinked, and CD71-crosslinked T cells, respectively. Panel **E** shows *P*-histogram of Bodipy-PC probe in control, untreated K6 T cells. The *M* values on all panels display the mean *P* value while the *w* values display the width of Gaussian from a Gauss-Marquardt fitting of data.

classic lipid markers of rafts could be observed on lymphoid and myeloid cells, as well as on other cell types, such as fibroblasts or heart muscle cells and did not show cell type-dependence. This might mean that, in contrast to model membrane systems, in live cells the raft domains may differ in their SM content and a fraction of diI may partition into SM-poor raft domains. Another alternative explanation is that the constitutive protein content of rafts may partially shield the molecular immiscibility of diIC18 and SM within these domains. Taking all these together, we can say that in live cells the Lo-Ld phase separation is likely smoothened relative to model membranes by the numerous proteins interacting with the lipid components of these domains.

The recently introduced DP-CLSM technique (25,26) proved to be useful so far in detecting macroscopic ultrastructural changes in different plant (membrane) structures using various measuring modalities offered by the method. Here we used the *P*-imaging modality of DP confocal microscopy and, by applying diIC18 probe, we concluded that technically DP-CLSM is capable of monitoring either probe orientations or pixel by pixel emission polarization heterogeneities all over the cell surface in intact lymphoid cells. While the statistical analysis of *P*-images for the fluid phase probe Bodipy-PC has shown a relatively narrow and quite depolarized *P*-distribution over tens of T lymphoma cells, the *P*-distributions for diIC18

were substantially broadened with a higher mean value. This can be accounted for by the contributions from *r* and possibly also from the existence of small scale ordered membrane regions (including partly rafts), as compared with B-PC which is homogenously labeling the fluid membrane regions.

Modification of lipid raft microdomains by either cholesterol depletion (domain disruption) or by crosslinking of raft-localized proteins, such as CD48 (domain aggregation), both sensitively influenced the *P*-distributions derived from *P*-images recorded on T cells. Aggregation of rafts through CD48 crosslinking and interestingly crosslinking of a nonraft protein transferrin receptor (CD71), both shifted the mean of the *P*-distribution toward a higher value (restricted rotational freedom). These changes might arise partially from the reduced rotational freedom of "raft-captured" diI molecules and/or from a dynamic coupling between the coalesced rafts and their partially ordered lipid neighborhood, where binding of diIC18 to certain proteins may increase upon their aggregation. Such phenomenon was reported earlier for FcεRI on mast cells, where antigens could induce a large scale coaggregation of lipids with the clustered receptors (43).

This mechanism, as a model of raft-mediated membrane reorganization was studied later in a relatively simple model membrane system (44) and it was shown that crosslinking of a raft lipid (such as G_{M1}) or a single raft protein (such as Thy1/
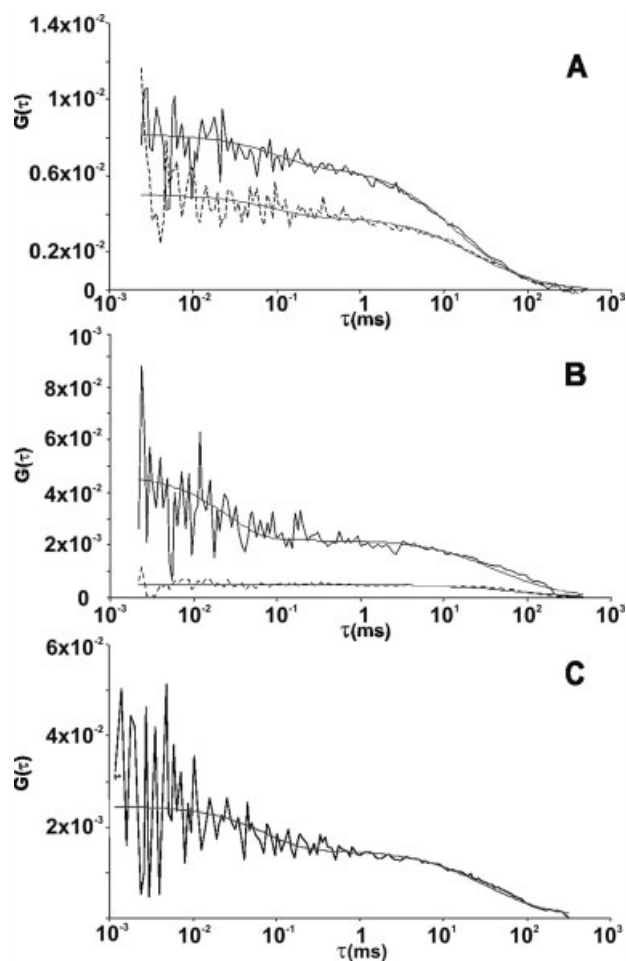
Figure 4. Fluorescence autocorrelation curves of diIC18(3) measured on Kit 225 K6 cells. For each sample $n \geq 10$ cells were measured; 10 runs lasting for 6 s each were carried out in every selected point. Presented curves are the averages of 10 runs. Representative curves from measurements on two control cells (**A**), two MBCD-treated cells (**B**), and one CD48 crosslinked cell (**C**) are shown. Autocorrelation curves were fitted to a model assuming a single free diffusion component and triplet correction (smooth curves). The average diffusion times for the control, MBCD-treated, and CD48-crosslinked samples were 24.1 ± 13.4, 62.9 ± 42, and 33.7 ± 7.8 ms, respectively.

CD90) may result in coexistence of phase separated Ld and Lo domains, at least in such models. Our DP-CLSM imaging data on diIC18 probe in live lymphocytes confirm that this might be an operating mechanism, when raft proteins, e.g. CD48 are crosslinked. The membrane reorganization induced by CD48 or CD71 crosslinking can also influence local diffusion properties of the investigated diIC18 probes either through the increased size of obstacles against their free diffusion or through an increase in the affinity of lipid–protein interaction upon protein aggregation, consistently with our present FCS microscopic data.

In conclusion, our data provided several pieces of evidence for protein compositional diversity of lipid rafts in live lymphoid cells. It was also shown that Lo (liquid ordered) domains defined by the diIC18 probe weakly overlap with the raft microdomains defined by $G_{M1,3}$ gangliosides and the new anti-cholesterol antibody reactive with clustered cholesterol. Finally, we demonstrated usefulness of the DP imaging in live human lymphoma cells. Using diIC18 probe, the *P*-images, in accordance with FCS microscopic data revealed a dynamic coupling between raft modulations and the neighboring lipid regions. To elucidate the mechanistic details of the latter, however, requires further analysis.

Literature Cited

1. Simons K, Ikonen E. Functional rafts in cell membranes. Nature 1997;387:569–572.
2. Edidin M. Shrinking patches and slippery rafts: Scales of domains in the plasma membrane. Trends Cell Biol 2001;11:492–496.
3. Matko J, Szöllősi J. Landing of immune receptors and signal proteins on lipid rafts: A safe way to be spatio-temporally coordinated? Immunol Lett 2002;82:3–15.
4. Horejsi V, Drbal K, Cebecauer M, Cerny J, Brdicka T, Angelisova P, Stockinger H. GPI microdomains: A role in signalling via immune receptors. Immunol Today 1999;20:356–361.
5. Alonso MA, Millán J. The role of lipid rafts in signaling and membrane trafficking in T lymphocytes. J Cell Sci 2001;114:3957–3965.
6. Matkó J, Szöllősi J. Regulatory apects of membrane microdomain (raft) dynamics in live cells: A biophysical approach. In: Mattson M, editor. Membrane Microdomain Signaling: Lipid Rafts in Biology and Medicine. Totowa, NJ: Humana Press; 2004. pp 15–46.
7. Rosenberger CM, Brumell JH, Finlay BB. Microbial pathogenesis: Lipid rafts as pathogen portals. Curr Biol 2000;10:R823–825.
8. Maekawa S, Iino S, Miyata S. Molecular characterization of detergent-insoluble cholesterol-rich membrane microdomain (raft) of the central nervous system. Biochim Biophys Acta 2003;1610:261–270.
9. Wolf Z, Orso E, Werner T, Klunemann HH, Schmitz G. Monocyte cholesterol homeostasis correlates with the presence of detergent resistant membrane microdomains. Cytometry A 2007;71A:486–494.
10. Grandl M, Bared SM, Liebisch G, Werner T, Barlage S, Schmitz G. E-LDL and Ox-LDL differentially regulate ceramide and cholesterol raft microdomains in human macrophages. Cytometry A 2006;69A:189–191.
11. Wu M, Holowka D, Craighead HD. Baird B. Visualization of plasma membrane compartmentalization with patterned lipid bilayers. Proc Natl Acad Sci USA 2004;101:13798–13803.
12. Edel JB, Wu M, Baird B, Craighead HG. High spatial resolution observation of single-molecule dynamics in living cell membranes. Biophys J 2005;88:L43–L45.
13. Kusumi A, Nakada C, Ritchie K, Murase K, Suzuki K, Murakoshi H, Kasai RS, Kondo J, Fujiwara T. Paradigm shift of the plasma membrane concept from the two-dimensional continuum fluid to the partitioned fluid: High-speed single-molecule tracking of membrane molecules. Annu Rev Biophys Biomol Struct 2005;34:351–378.
14. Kahya N, Schwille P. Fluorescence correlation studies of lipid domains in model membranes. Mol Membr Biol 2006;23:29–39.
15. Brock R, Vámosi G, Vereb G, Jovin TM. Rapid characterization of green fluorescent protein fusion proteins on the molecular and cellular level by fluorescence correlation microscopy. Proc Natl Acad Sci USA 1999;96:10123–10128.
16. Parasassi T, Gratton E, Yu WM, Wilson P, Levi M. Two-photon fluorescence microscopy of laurdan generalized polarization domains in model and natural membranes. Biophys J 1997;72:2413–2429.
17. Lawrence JC, Saslowsky DE, Edwardson JM, Henderson RM. Real-time analysis of the effects of cholesterol on lipid rafts behavior using atomic force microscopy. Biophys J 2003;84:1827–1832.
18. Giocondi M-C, Milhiet PE, Dosset P, Grimellec CL. Use of cyclodextrin for AFM monitoring of model raft formation. Biophys J 2004;86:861–869.
19. Biro A, Cervenak L, Balogh A, Lorincz A, Uray K, Horvath A, Romics L, Matko J, Fust G, Laszlo G. Novel anti-cholesterol monoclonal IgG antibodies as probes and potential modulators of membrane raft-dependent immune functions. J Lipid Res 2007;48:19–29.
20. Korlach J, Schwille P, Webb WW, Feigenson GW. Characterization of lipid bilayer phases by confocal microscopy and fluorescence correlation spectroscopy. Proc Natl Acad Sci USA 1999;96:8461–8466.

New Faces of Membrane Microdomains

21. Feigenson GW, Buboltz JT. Ternary phase diagram of dipalmitoyl-PC/dilauroyl-PC/cholesterol: Nanoscopic domain formation driven by cholesterol. Biophys J 2001;80:2775–2788.

22. Bacia K, Schwille P, Kurzchalia T. Sterol structure determines the separation of phases and the curvature of the liquid-ordered phase in model membranes. Proc Natl Acad Sci USA 2005;102:3272–3277.

23. Kahya N, Scherfeld D, Bacia K, Poolman B, Schwille P. Probing lipid mobility of raft-exhibiting model membranes by fluorescence correlation spectroscopy. J Biol Chem 2003;278:28109–28115.

24. Bacia K, Scherfeld D, Kahya N, Schwille P. Fluorescence correlation spectroscopy relates rafts in model and native membranes. Biophys J 2004;87:1034–1043.

25. Garab G, Pomozi I, Jörgens R, Weiss G. Method and apparatus for determining the polarization properties of light emitted, reflected or transmitted by a material using a laser scanning microscope. U.S. Pat. 6,856,391 (2005).

26. Steinbach G, Pomozi I, Zsiros O, Garab G. Imaging fluorescence detected linear dichroism and emission anisotropy of plant cell walls in laser scanning confocal microscope. Cytometry A 2008; in press (this issue).

27. Axelrod D. Carbocyanine dye orientation in red cell membrane studied by microscopic fluorescence polarization. Biophys J 1979;26:557–573.

28. Matko J, Bodnár A, Vereb G, Bene L, Vámosi G, Szentesi G, Szöllősi J, Horejsi V, Waldmann TA, Damjanovich S. GPI-microdomains (membrane rafts) and signaling of the multichain interleukin-2 receptor in human lymphoma/leukemia T cell lines. Eur J Biochem 2002;269:1199–1208.

29. Spits H, de Vries JE, Terhorst C. A permanent human cytotoxic T-cell line with high killing capacity against a lymphoblastoid B-cell line shows preference for HLA A. B target antigens and lacks spontaneous cytotoxic activity. Cell Immunol 1981;59:435–447.

30. Gombos I, Detre C, Vamosi G, Matko J. Rafting MHC-II domains in the APC (presynaptic) plasma membrane and the thresholds for T-cell activation and immunological synapse formation. Immunol Lett 2004;92:117–124.

31. Szöllősi J, Matko J, Vereb G. Cytometry of fluorescence resonance energy transfer (FRET). In: Darzynkiewicz Z, Roederer M, Tanke H, editors. Methods in Cell Biology 2004;75:105–152.

32. Nagy P, Vámosi G, Bodnár A, Lockett SJ, Szöllösi J. Intensity-based energy transfer measurements in digital imaging microscopy. Eur Biophys J 1998;27:377–389.

33. Vámosi G, Bodnár A, Vereb G, Jenei A, Goldman CK, Langowski J, Tóth K, Mátyus L, Szöllősi J, Waldmann TA, Damjanovich S. IL-2 and IL-15 receptor alpha-subunits are coexpressed in a supramolecular receptor cluster in lipid rafts of T cells. Proc Natl Acad Sci USA 2004;101:11082–11087.

34. Wachsmuth M, Waldeck W, Langowski J. Anomalous diffusion of fluorescent probes inside living cell nuclei investigated by spatially-resolved fluorescence correlation spectroscopy. J Mol Biol 2000;298:677–689.

35. Gombos I, Bacsó Zs, Detre C, Nagy H, Goda K, Andrásfalvy M, Szabó G, Matkó J. Cholesterol-sensitivity of detergent resistance: A rapid flow cytometric test for detecting constitutive or induced raft association of membrane proteins. Cytometry A 2004;61A:117–126.

36. Poloso NJ, Roche PA. Association of MHC class II-peptide complexes with plasma membrane lipid microdomains. Curr Opin Immunol 2004;16:103–107.

37. Bodnár A, Bacsó Z, Jenei A, Jovin TM, Damjanovich S, Edidin M, Matkó J. Class I HLA oligomerization at the surface of B cells is controlled by exogenous β2-microglobulin: implications in activation of cytotoxic T lymphocytes. Int Immunol 2003;15:331–339.

38. Garab G. Linear and circular dichroism. In: Amesz J, Hoff A, editors. Biophysical Techniques in Photosynthesis. Dordrecht: Kluwer; 1996. pp. 11–40.

39. Bouillon M, El-Fakhry Y, Girouard J, Khalil H, Thibodeau J, Mourad W. Lipid raft-dependent and -independent signaling through HLA-DR molecules. J Biol Chem 2003;278:7099–7107.

40. Legembre P, Daburon S, Moreau P, Moreau JF, Taupin JL. Modulation of Fas mediated apoptosis by lipid rafts in T-lymphocytes. J Immunol 2006;176:716–720.

41. Drobnik W, Borsukova H, Böttcher A, Pfeiffer A, Liebisch G, Schütz GJ, Schindler H, Schmitz G. Apo AI/ABCA-1-dependent and HDL-3 mediated lipid efflux from compositionally distinct cholesterol-based microdomains. Traffic 2002;3:268–278.

42. Mendez AJ, Lin G, Wade DP, Lawn RM, Oram JF. Membrane lipid domains distinct from cholesterol/sphingomyelin-rich rafts are involved in the ABCA1-mediated lipid secretory pathway. J Biol Chem 2001;276:3158–3166.

43. Thomas JL, Holowka D, Baird B, Webb WW. Large-scale co-aggregation of fluorescent lipid probes with cell surface proteins. J Cell Biol 1994;125:795–802.

44. Dietrich C, Volovyk ZN, Levi M, Thompson NL, Jacobson K. Partitioning of Thy-1. GM1 and crosslinked phospholipid analogs into lipid rafts reconstituted in supported model membrane monolayers. Proc Natl Acad Sci USA 2001;98:10642–10647.